Separation and Purification Technology 361 (2025) 131497

Contents lists available at ScienceDirect

Separation and Purification Technology

journal homepage: www.elsevier.com/locate/seppur

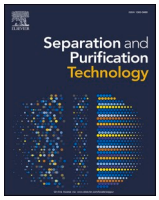

Separation of nonracemic mixtures of enantiomers by achiral simulated moving bed chromatography

Wojciech Kazimierz Marek [a,*], Ju Weon Lee [b], Andreas Seidel-Morgenstern [b], Dorota Antos [a,*]

[a] Department of Chemical and Process Engineering, Rzeszów University of Technology, Powstańców Warszawy Ave. 6, 35-959 Rzeszów, Poland
[b] Max Planck Institute for Dynamics of Complex Technical Systems, Sandtorstrasse 1, 39106 Magdeburg, Germany

ARTICLE INFO

Keywords:
Enantiomer separation
Simulated moving bed
Self-disproportionation of enantiomers
Achiral chromatography

ABSTRACT

A continuous process for isolating pure enantiomers from nonracemic mixtures by achiral multicolumn chromatography has been developed. The mechanism of the separation was based on self-disproportionation of enantiomers (SDE). This phenomenon relies on the formation of homochiral and heterochiral associates that differ in adsorption behavior. A standard four-zone simulated moving bed (SMB) unit was exploited for process realization, in which the target enantiomer was collected in the raffinate outlet, and the unresolved fraction of both enantiomers was collected in the extract outlet. Separation was performed in silica gel columns for a model mixture of methyl *p*–tolyl sulfoxide enantiomers, in which S–methyl *p*–tolyl sulfoxide was the target enantiomer. Systematic experiments were performed to assess the influence of the operating conditions on the process performance, including the flowrates in the SMB zones, the switching time, the feed concentration, and the enantiomeric excess of the feed mixture. The product yield obtained in the experimental runs varied from 14 to 73%, the purity from 81% to 100%, and the productivity from 15 to 99 g per liter of the total column volume per day. The process design was supported by a mathematical model that accounted for the specificity of the SDE-driven separation. The process was found to be feasible, reproducible, and predictable. It can be applied in industrial production to isolate the target enantiomer from nonracemic mixtures obtained from asymmetric synthesis and is seen as an attractive alternative to enantioselective chromatography using expensive chiral stationary phases.

1. Introduction

Currently, chiral drugs represent more than 70 % of the drug market [1]. The chirality of a drug determines the biological activity, safety, and efficacy. In 1992, the Food & Drug Administration (FDA) published a series of guidelines for the pharmaceutical development of chiral drugs imposed the obligation to pharmacologically profile both racemate and individual enantiomers, as well as a regulatory preference to bring a single enantiomer to the market [2]. Since then, in addition to the development of new pure enantiomers into a therapy, the 'chiral switch' strategy, which consists of switching from the existing racemate to one of its optical isomers, has emerged to improve the safety and efficacy of existing agents [3–7].

The interest in the production of pure enantiomers is not only restricted to the pharmaceutical industry, but also impacts the production of food and agrochemicals [8,9]. Chiral pesticide production is expected to grow significantly [9], which can drive the global demand for chiral compounds in the near future. To meet this challenge, new cost-effective manufacturing techniques are required.

To produce a single enantiomer, two main approaches are available that involve asymmetric or symmetric synthesis [10–13]. The former is the most straightforward; however, it requires efficient catalysts to allow for enantioselective reactions. Asymmetric synthesis rarely provides a target enantiomer with desired purity, but instead a nonracemic mixture with a certain enantiomeric excess (*ee*) that has to be further separated in the presence of a chiral selector. Symmetric synthesis provides a racemic mixture of two enantiomers. As it does not require a chiral environment, it is usually economically more attractive than asymmetric synthesis [14]. Nevertheless, in the next step, the racemic mixture is resolved in a chiral environment.

Several techniques can be used for the chiral separation of enantiomers from postsynthesis mixtures, among which chiral chromatography (CCh) and diastereoisomeric crystallization are considered straightforward and easy to perform on a large scale [15,16,17]. Diastereoisomeric

* Corresponding authors.
E-mail addresses: wmarek@prz.edu.pl (W.K. Marek), dorota.antos@prz.edu.pl (D. Antos).

https://doi.org/10.1016/j.seppur.2025.131497
Received 9 December 2024; Accepted 6 January 2025
Available online 10 January 2025

crystallization is economically attractive; however, its realization requires the use of suitable chiral resolving agents. The identification of efficient resolving agents that allow the formation of pure crystals of the target enantiomer is often very problematic due to the diversity and complexity of the solid phase behavior of enantiomeric mixtures [18]. Furthermore, diastereoisomeric crystallization is not feasible for chiral compounds that do not occur in crystalline form. Considering the above aspects, CCh is seen as easier to realize because there is a large arsenal of chiral stationary phases (CSPs) commercially available, which enables the separation of a wide variety of chiral compounds. However, because of the high prizes of CSPs, CCh is a cost driver in the manufacturing of enantiomers. Furthermore, there are often processing limitations regarding mechanical stability of CSP. Finally, the chromatographic throughput is limited by the binding capacity of the CSPs, making CCh a bottleneck in the production process on a large scale.

To mitigate this issue, the continuous simulated moving bed technique (SMB) can be applied. It offers improvement compared to batch-wise separations. The classical SMB process is well understood and criteria to design this technique have already been developed in the 1990s [19–21]. A standard SMB unit consists of two separation zones and two regeneration zones, which contain several chromatographic columns connected in series. A mixture of two compounds to be separated is continuously delivered into the feed inlet, whereas the regenerating agent (desorbent) is continuously delivered into the desorbent inlet. Strongly and weakly retained compounds are transported in opposite directions by the simulated countercurrent movement of the solid phase and the mobile phase and can be individually collected at specific extract and raffinate outlets, respectively. Such a configuration is, in particular, suitable for the separation of binary mixtures. Therefore, it suits very well for separating mixtures of enantiomers. The possibility of chiral separation of enantiomeric mixtures by the use of the SMB technique or its modifications has been demonstrated in a number of studies [22–31]. In each of these studies, the SMB separation performed better than the batch-wise separation with respect to yield, purity, and productivity. Despite these advantages, the issue of high costs for CSPs persisted. Partial or complete replacement of CCh by achiral chromatography (ACh), which is significantly cheaper to realize, could potentially improve the process economy and reduce the number of process development stages, and thus the time to deliver the product to the market.

Despite the identical physicochemical properties of enantiomers, their chromatographic separation in an achiral environment is possible. The phenomenon that can be exploited was introduced as the self-disproportionation of enantiomers (SDE) [32]. SDE results from asymmetric interactions of enantiomers, which induce formation of homo- and hetero-chiral associates with different adsorption properties. This allows isolation of the enantiomer having a higher *ee* in the nonracemic mixture using an achiral adsorbent, such as plane silica.

SDE was shown to occur for different classes of chiral compounds that possess the so-called SDE-phoric groups, including sulfoxides, CF_3-derived substances, amides, carboxylic acids, amino acids, dipeptide derivatives, alcohols, phenols, esters, heterocycles [32–41].

In our previous study, we have developed a mechanistic model to quantitatively describe SDE-driven chromatographic separation. The model was used to assess the efficiency of the separation of various enantiomeric mixtures in a plane silica column in isocratic and gradient elution modes [42,43].

In this study, to improve the economics of the process and make it applicable on an industrial scale, we have developed a novel approach for continuous separation of enantiomers by achiral SMB (ACh–SMB). In this process, the enantiomer with a higher *ee* in the feed stream is collected as a pure compound at the raffinate outlet, whereas the unresolved fraction of both enantiomers is collected at the extract outlet.

The general goal of the study was to verify the feasibility, repeatability, and predictability of the ACh–SMB concept. For this purpose, a series of ACh–SMB runs were performed for a chiral model system, namely methyl *p*–tolyl sulfoxide (MTSO) enantiomers, exploiting standard silica gel columns. The influence of important operating parameters on the separation performance of a target enantiomer (*S*–MTSO) was examined theoretically and experimentally, focusing on SMB zone flowrates, the concentration and *ee* of the feed mixtures. To prove predictability of separation performance, a dynamic model was formulated and calibrated on the basis of experimental data.

2. Theory

2.1. Principles of SDE-driven separation

As mentioned above, separation of nonracemic mixtures of enantiomers in ACh–SMB is driven by the SDE-phenomenon, i.e., by the formation of homochiral associates between molecules of the same enantiomers and heterochiral associates between molecules of the opposite enantiomers. It is assumed that the formation of associates occurs in the adsorbed phase according to the following reaction paths [42,43]:

- interaction of enantiomer i with an active site S^* on the bare adsorbent surface in layer I:

$$E_i + S^* \Leftrightarrow E_i S^* \tag{1}$$

- interaction with an active site provided by the molecule of the same enantiomer ($i = j$) to form a homochiral associate or the opposite enantiomer ($i \neq j$) to form a heterochiral associate in layer II:

$$E_i + E_j S^* \Leftrightarrow E_i E_j S^* \tag{2}$$

At adsorption equilibrium, the total adsorption of the enantiomer i, $q^*_{i,tot}$, can be expressed as follows [42,43]:

$$\begin{aligned} q^*_{i,tot} &= q_i^{*I} + q_i^{*II} \\ &= \frac{q^m K^I C_i}{1 + K^I \sum_i C_i} + \frac{q_i^{*I} K^{II}_{hom} C_i}{1 + K^{II}_{hom} C_i + K^{II}_{het} C_j} + \frac{q_j^{*I} K^{II}_{het} C_i}{1 + K^{II}_{het} C_i + K^{II}_{hom} C_j} \end{aligned} \tag{3}$$

The first term on the right-hand side corresponds to adsorption on bare silica, the second and third terms correspond to adsorption of homochiral and heterochiral associates, respectively, q^m is the binding capacity on bare silica, and K^I is the corresponding equilibrium constant, which both are the same for both enantiomers on an achiral bare silica surface: $K^I_i = K^I_j = K^I$ and $q^m_i = q^m_j = q^m$, K^{II}_{hom}, K^{II}_{het} are the equilibrium constants of binding of the enantiomer on the adsorption sites provided by the molecules of the same enantiomer and the opposite enantiomer, respectively. The energy of the formation of heterochiral and homochiral associates is different $K^{II}_{hom} \neq K^{II}_{het}$, which is a cause of their different retention behavior in nonracemic mixtures.

For low concentrations, q_i^{*II} tends to zero, and Eq. (3) converts to the linear isotherm:

$$q_i^{*I} = HC_i \tag{4}$$

where H is the Henry constant equivalent to the initial isotherm slope:

$$H = q^m K^I \tag{5}$$

Under linear isotherm conditions, the Henry constant determines the migration velocity of band profiles along the column. Since the isotherm slopes of both enantiomers are identical on achiral stationary phase, their separation is not possible in the linear isotherm range.

For racemic mixtures, the concentrations of enantiomers in the liquid phase are the same ($C_i = C_j$), hence their concentrations in the adsorbed phase are also the same ($q^*_{i,tot} = q^*_{j,tot}$). Therefore, for racemic mixtures, separation of the two enantiomers is also not possible, regardless of the

feed concentration and the isotherm range covered.

The separation of enantiomers is feasible only for nonracemic mixtures under nonlinear isotherm conditions, for which the fronts of their band profiles move with different velocities. These velocities are determined by the isotherm chord, which connects the feed concentration and the origin. The slope of the isotherm chord of the target enantiomer, which is in excess in the nonracemic mixture, is lower than that for the enantiomer in depletion; therefore, its concentration front migrates through the column faster. The distance between the fronts of the enantiomers allows collecting a fraction of the pure product. The idea behind the SDE-driven separation of enantiomers, which is the basis of the ACh–SMB process developed in this study, is illustrated in Fig. 1.

2.2. ACh-SMB concept

The concept of the ACh–SMB is illustrated in Fig. 2. The arrangement of the ACh–SMB unit is similar to that of a standard SMB unit (Fig. 2A). A binary mixture with an excess of the target enantiomer (*E*1) compared to the undesired enantiomer (*E*2) is delivered to the feed inlet (*F*) between zones 2 and 3. The desorbent is delivered to zone 1 at the desorbent inlet (*D*) to regenerate the stationary phase. The fraction of the pure enantiomer *E*1, whose concentration front migrates with higher velocity compared to the enantiomer *E*2, is collected at the raffinate outlet (Fig. 2B). The unresolved fraction of both enantiomers is collected at the extract outlet (*Ex*). In the open-loop arrangement used in this study, the liquid phase that leaves zone 4 (*Z*) is discarded. Therefore, the cross-contamination of zone 1 by the undesired enantiomer *E*2 that leaks out of zone 4 is avoided. This makes the open-loop arrangement easier to perform compared to the closed-loop arrangement, in which effluent from zone 4 is recycled to zone 1, so cross-contamination can occur. Therefore, realization of the separation in an open-loop arrangement may be preferable in the process design stage. The rules for the design of the standard SMB process are based on the so-called triangle theory [21]. However, the design of an ACh–SMB separation requires the development of a new procedure, which accounts for the specificity of the SDE phenomena. As mentioned above, SDE-driven separation is not possible in the linear isotherm range, for which the Henry constants of both opposite enantiomers are the same. Hence, the process design cannot be based on triangle theory, in which Henry constants are used to define the location of the operating space [21].

2.3. Design of the ACh-SMB process

The process design can be based on the determination of the space of the operating variables, which are defined using dimensionless flowrates in each of the four zones (m^n) [21]:

$$m^n = \frac{Q^n t_{sw} - V_{col}\varepsilon_t}{V_{col}(1-\varepsilon_t)} \qquad n = 1,..,4 \tag{6}$$

where V_{col} is the column volume, Q^n is the liquid phase flowrate in n-th zone, t_{sw} is the switching time defined as:

$$t_{sw} = \frac{V_{col}(1-\varepsilon_t)}{Q_s} \tag{7}$$

where Q_s is the simulated flowrate of the solid phase, ε_t is the packed bed total porosity.

The values of m^n determine the dimensionless flowrates in the feed, *F*, raffinate, *Ra*, and extract, *Ex* streams, according to the overall mass balances:

$$m_{Feed} = m^3 - m^2 > 0 \tag{8}$$

$$m_{Ra} = m^3 - m^4 > 0 \tag{9}$$

$$m_{Ex} = m^1 - m^2 > 0 \tag{10}$$

2.4. Dynamic model

The design of ACh–SMB can be aided by mathematical modelling. For this purpose, we used the equilibrium-dispersive model [44]:

$$\frac{\partial C_i}{\partial t} + F\frac{\partial q^*_{i,tot}}{\partial t} + \frac{u}{\varepsilon_t}\frac{\partial C_i}{\partial x} = D_{ap}\frac{\partial^2 C_i}{\partial x^2} \qquad i = E1, E2 \tag{11}$$

where $q^*_{i,tot}$ is the equilibrium concentration in the adsorbed phase in grams of the species i per liter of the solid matrix (g/L_{matrix}) given by the isotherm equation (Eq. 3), C_i (g/L) is the concentration of the liquid phase, t (s), x (m) are the time and spatial coordinates, respectively, u (m/s) is the superficial velocity, $F = (1-\varepsilon_t)/\varepsilon_t$ is the phase ratio, D_{ap} (m^2/s) is the apparent dispersion coefficient correlated with the number of theoretical plates, *N*, according to:

$$\frac{uL}{D_a\varepsilon_t} = \frac{N}{2} \tag{12}$$

The model is coupled with the following initial condition:

$$C_i^n(x, t=0) = 0, n = 1,...,4,\ i = E1, E2 \tag{13}$$

which corresponds to the columns that are initially not preloaded with the enantiomers. The boundary conditions at the column inlets ($x = 0$) and outlets ($x = L$) are defined for each column and each zone ($n =$

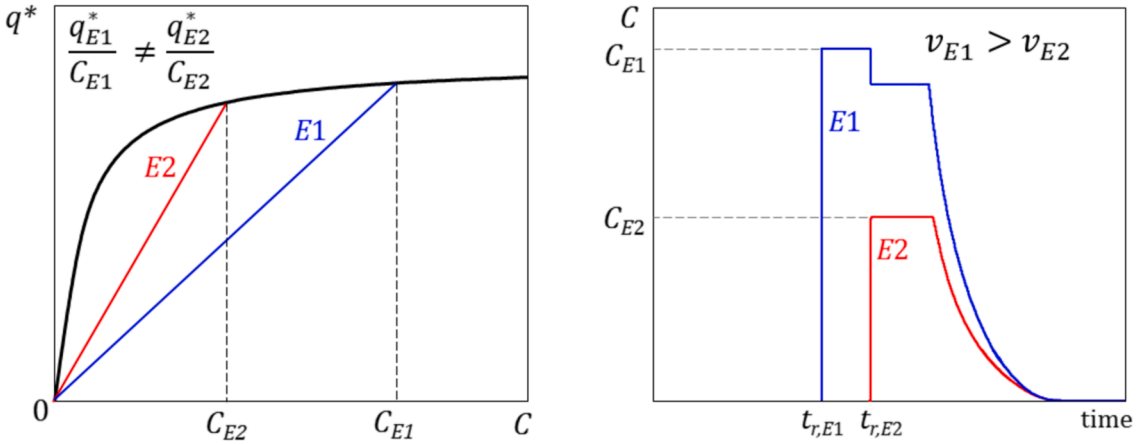

Fig. 1. Illustration of the principles of SDE-driven separations, $\frac{q^*_{Ei}}{C_{Ei}}$ is the isotherm chord, v_i is the migration velocity of the concentration front, $v_i = \frac{u}{\varepsilon_t}/\left(1+(1-\varepsilon_t)/\varepsilon_t\frac{q^*_{Ei}}{C_{Ei}}\right)$, where u is the superficial velocity and ε_t is the total adsorbent porosity.

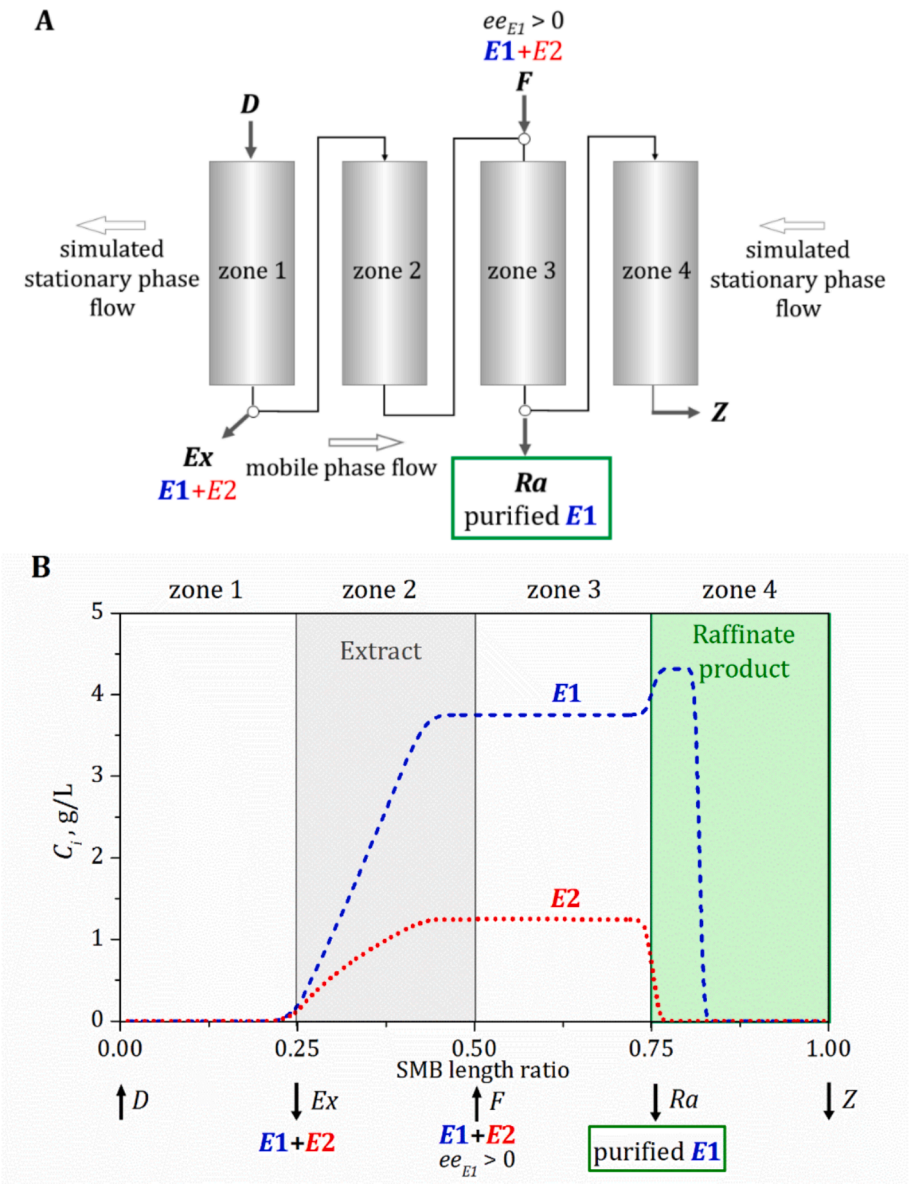

Fig. 2. Illustration of the separation concept of enantiomers in the ACh–SMB unit. (A) Configuration of the SMB unit and (B) illustration of the internal profiles of enantiomers in an SDE-driven SMB separation for feed enriched with *E*1 ($ee_{E1} > 0$).

1,…,4) as follows:

$$C_{i,in}^{n=1}(x=0,t)=0 \tag{14}$$

$$C_{i,in}^{n=3}(x=0,t)=\frac{C_{i,out}^{n=2}(x=L,t)Q^{n=2}+C_{i,F}Q_F}{Q^{n=3}} \tag{15}$$

$$C_{i,in}^{n}(x=0,t)=C_{i,out}^{n-1}(x=L,t) \qquad n=2,4 \tag{16}$$

$$\frac{\partial C_i^n(x=L,t)}{\partial t}=0 \qquad n=1,\ldots,4 \tag{17}$$

The model was preliminarily calibrated using a batch column (section 4.1). In this case, the following boundary condition was used at the column inlet:

$$C_i(x=0,t<t_{inj})=C_{i,F}, C_i(x=0,t>t_{inj})=0 \tag{18}$$

where t_{inj} is the injection time.

For the boundary condition at the outlet of the batch column Eq. (17) was applied.

To solve Eq. (11), along with the corresponding initial and boundary conditions, a fast finite difference algorithm based on the method developed by Rouchon was used [45]. Both the model and the solution method are sufficiently accurate in the simulation of chromatography processes in HPLC columns, which are typically used for such separation types. The method provides concentration profiles for the steady-state solution of the SMB process in a very short calculation time [46]. This is advantageous when the model needs to be calibrated by adjusting several parameters required for screening the operating space and used for process optimization.

2.5. Determination of the performance indicators

To quantify the performance of the ACh–SMB separation, different indicators were determined, including: productivity, yield, product purity and its average concentration, and eluent consumption.

The productivity of the target enantiomer, which is in excess in the enantiomeric mixture, Pr_{E1}, is expressed as:

$$Pr_{E1,Ra} = \frac{\overline{C_{E1,Ra}}\, Q_{Ra}}{4V_{col}} \tag{19}$$

where $\overline{C_{E1,Ra}}$ is the average concentration of $E1$ collected at the raffinate outlet during the switching time in steady state. It is calculated by integrating the local concentration profile, $C_{E1,Ra}(t)$, over the switching time:

$$\overline{C_{E1,Ra}} = \frac{\int_t^{t+t_{sw}} C_{E1,Ra}(t)dt}{t_{sw}} \tag{20}$$

The separation yield is defined as the ratio of the mass of the purified product, i.e. the target enantiomer, *E1,* in the raffinate stream, to its mass delivered with the feed stream:

$$Y_{E1,Ra} = \frac{\overline{C_{E1,Ra}} Q_{Ra}}{C_{E1,F} Q_F} 100\% \tag{21}$$

The purity of the target enantiomer in the product stream is defined as follows:

$$Pu_{E1,Ra} = \frac{\overline{C_{E1,Ra}}}{\overline{C_{E1,Ra}} + \overline{C_{E2,Ra}}} 100\% \tag{22}$$

where $\overline{C_{E2,Ra}}$ is the average concentration of the undesired enantiomer $E2$, determined analogously to Eq. (20).

The eluent consumption (EC), which is another cost-generating factor, is defined as a ratio of the volumetric flow of the feed and desorbent inlet streams to the mass flow of the product:

$$\mathrm{EC} = \frac{Q_D + Q_F}{Q_{Ra}\overline{C_{E1,Ra}}} \tag{23}$$

3. Experimental

3.1. Equipment

The ACh–SMB system consisted of four Smartline Pumps 100 V.5010, two UV-detectors (K-2501), SMB-Control unit and multifunctional valve (CSEP C9 Series Simulated Moving Bed and Chromatography Systems V0499, 12/2000), from Knauer (Berlin, Germany).

Chromatographic batch experiments were performed using an HPLC system (JASCO, Tokyo, Japan) with the PDA detector MD-4010 and the multicolumn thermostat CO-4065.

The Dionex Ultimate 3000 HPLC system with the PDA detector and Chromeleon software (Thermo Scientific, Germering, Germany) was used for the offline concentration analysis of the enantiomers.

3.2. Materials

HPLC gradient grade solvents: propan-2-ol (*i*-PrOH) and methyl *tert*-butyl ether (MTBE), were purchased from VWR Chemicals, Germany.

The model enantiomeric mixture consisted of *S*–(−)methyl *p*–tolyl sulfoxide (*S*–MTSO) CAS 5056–07-5, which was the target enantiomer (*E*1), and *R*–(+)methyl *p*–tolyl sulfoxide (*R*–MTSO), CAS: 1519–39-7. *S*–MTSO (Pu > 98 %) was provided by AmBeed (Arlington Heights, USA), the racemic mixture *R*,*S*–MTSO (Pu > 99 %) was provided by Apollo Scientific (Bredbury, UK). *R*,*S*–MTSO and *S*–MTSO were pre-purified by flash silica gel chromatography and recrystallization to remove an undefined strongly adsorbing impurity, whose presence in the provided material caused contamination of the columns in a long term use.

Achiral separations of the MTSO enantiomers in the batch column and the ACh–SMB unit were performed using conventional silica columns. In the study, four ReproSil 70 Silica columns 250x4 mm with a particle size of 15 μm (Dr. Meisch, Ammerbuch, Germany) were used. The total column volume of all columns connected in the SMB unit added up to 12.6 mL.

The concentration analysis of the enantiomeric mixtures was performed using the CHIRALPAK® IC column 250 × 4.6 mm, with a particle size of 5 μm (Daicel Corporation, Osaka, Japan).

3.3. Procedures

3.3.1. Preliminary batch separation

The condition for batchwise achiral separation of the MTSO enantiomers was optimized in a previous study [43]. Samples of the enantiomeric mixtures were prepared by mixing *S*–MTSO and *R*,*S*–MTSO in adequate proportions and dissolving the obtained mixture in the mobile phase, to obtain the total concentration of the enantiomers 60 g/L with $ee_S = 50$ % (i.e. $C_S = 45$ g/L and $C_R = 15$ g/L). Separation was performed in a normal phase system with a mobile phase composed of a 3 % v/v solution of *i*-PrOH in nonpolar MTBE. A 30 μL volume sample was injected into the ReproSil 70 Silica columns and isocratically eluted with the mobile phase. The mobile phase flowrate was 1 mL/min. Individual profiles of the enantiomers in the mixtures were determined by fractionation of column effluent and subsequent offline analysis of the fractions by chiral chromatography (section 3.3.3). The volume of fraction was changed from 0.2 to 1 mL; the sampling rate was adjusted to the pace of changes in the detector signal.

3.3.2. ACh-SMB separations

As mentioned above, the ACh–SMB experiments were performed in the open-loop arrangement in a typical four–zone SMB system illustrated in Fig. 2. Simulated movement of the stationary phase was realized by switching the position of the columns in the 16–port multi-way valve in countercurrent direction to the mobile phase flow. The frequency of shifts was specified by the switching time (t_{sw}). At the outlet of the raffinate and extract pumps, back pressure regulators (~1 MPa) were installed to enable stable and accurate pump work. The total extra-column volume of the SMB unit, i.e., volume of connection capillaries and valves, was 0.4 mL as determined on the basis of the geometry of the system elements.

Different total concentrations of the MTSO enantiomers and different enantiomeric compositions in the feed stream were used for the experimental runs: $C_F = 3$, 5 or 7 g/L and $ee_S = 30$, 50 or 70 %. The flowrates in the four zones (Q^1, Q^2, Q^3, Q^4) were varied between 1 and 3 mL/min. A maximum flowrate 3 mL/min was assigned to zone 1 in which the desorbent was delivered $Q^1 = Q_D$. This maximum flowrate was set due to the allowable pressure drop in the SMB unit (max. 9 MPa). The zone flowrates determined the flowrates of the feed, extract and raffinate streams (Q_F, Q_{Ex}, Q_{Ra}). The profiles at the raffinate and extract outlets were controlled by two online UV detectors.

The effluent fractions were collected at the extract (*Ex*) and raffinate (*Ra*) outlets during a single switch and during whole cycles consisting of 4 switches and subjected to concentration analysis of both enantiomers (section 3.3.3).

Cyclic steady states of the process were achieved after approx. 11 cycles when the columns were not initially preloaded with the enantiomers or after approx. 5 cycles when the columns already preloaded with enantiomers were used from run to run (Supplementary materials, Figs. S1 and S2).

3.3.3. Fraction analysis by chiral HPLC

The analysis of fractions acquired from the batch column and the SMB unit was performed using the CHIRALPAK® IC column assembled in the Dionex chromatographic system. The mobile phase was composed of 15 % v/v *i*-PrOH in MTBE, the mobile phase flowrate was 1.5 mL/min. The profiles were recorded at wavelengths of 244 nm (higher sensitivity to UV signal) for low sample concentrations and 270 nm (lower sensitivity to UV signal) for high sample concentrations. The concentration of the individual enantiomers in the fractions was calculated on the basis of the calibration curve of the standard samples. The calibration curves were linear in the concentration ranges used.

3.3.4. Determination of the column porosity and the apparent dispersion coefficient

To determine the porosity of the columns, a 5 μL pulse of hexane (a tracer) was eluted from the column under nonadsorbing conditions (100 % *i*-PrOH as the mobile phase). The retention time of the pulse (t_r) was reduced by the retention time in extra-column volumes, i.e., the volume of the injection line without the column, and used to calculate the total column porosity ε_t from the following formula:

$$t_r = \frac{V_{col}\varepsilon_t}{Q} \tag{24}$$

The apparent dispersion coefficient was determined from the number of theoretical plates, N (Eq. (12)) calculated from the second central moment of a small pulse of MTSO racemate at the flowrates changed in the range 1–3 mL/min with 3 % v/v *i*-PrOH in MTBE as the mobile phase. These measurements were repeated for all four columns to evaluate their similarity. The deviations from the mean N value between the columns did not exceed 5 %.

4. Results and discussion

4.1. Development of ACh-SMB process

4.1.1. Design concept

As mentioned above, triangle theory as the classical design tool ([21]) does not apply to SDE-driven separation, since the Henry constants of the enantiomers are the same. Therefore, the realization of the ACh–SMB process required the development of a new design procedure. It consisted of three steps as follows:

- batch-column separation of enantiomers for preliminary calibration of the dynamic model to estimate isotherm parameters,
- model-aided selection of the operation variables for identifying conditions for a first scouting ACh–SMB experiment,
- adjusting experimentally relevant ACh–SMB operating conditions to evaluate process performance.

4.1.2. Model calibration

Only very few elution experiments were sufficient for the evaluation of the model parameters (Eqs. 3, 11): total column porosity, ε_t, apparent dispersion coefficient, D_a, and the isotherm coefficients $q^m, K^I, K^{II}_{hom}, K^{II}_{het}$.

The value of ε_t was determined for all four columns from the retention time of the tracer pulse (section 3.3.4). The average value of ε_t was equal 0.70; the deviation from that value between the columns did not exceed 1 %.

The number of theoretical plates was measured as described in section 3.3.4. For the flowrate range 1–3 mL/min and for all columns, the mean value of approximately $N = 1000$ was determined and used to determine D_a (Eq. (17). Since the process was carried out under conditions of strong isotherm nonlinearity, for which thermodynamic effects dominated retention behavior, the accuracy of the ACh-SMB simulations was not sensitive to the plate number greater than 1000.

The isotherm coefficients were estimated on the basis of the concentration profiles of the enantiomeric mixture measured in the batch column separation (section 3.3.1). Column loading was selected to ensure that the SDE phenomenon was active, which was demonstrated by the presence of dual maxima on the UV chromatograms recorded for nonracemic mixtures (Fig. 3). To determine the individual profiles of the enantiomers, the column effluent was fractionated and subjected to concentration analysis using the chiral column (section 3.3.3). In the next step, the peak fitting method ([44]) was used to estimate the isotherm coefficients. The dynamic model coupled with the isotherm equation was implemented in a random search optimization procedure, which minimized the squared differences between the model simulations and the individual concentration profiles of the enantiomers by adjusting the isotherm parameters. The estimation results and the corresponding experimental concentration profiles are depicted in Fig. 3, and the isotherm coefficients obtained are presented in Table 1. These estimated model parameters were then adjusted to match the experimental results obtained in the ACh–SMB experiments, as described in section 4.3.

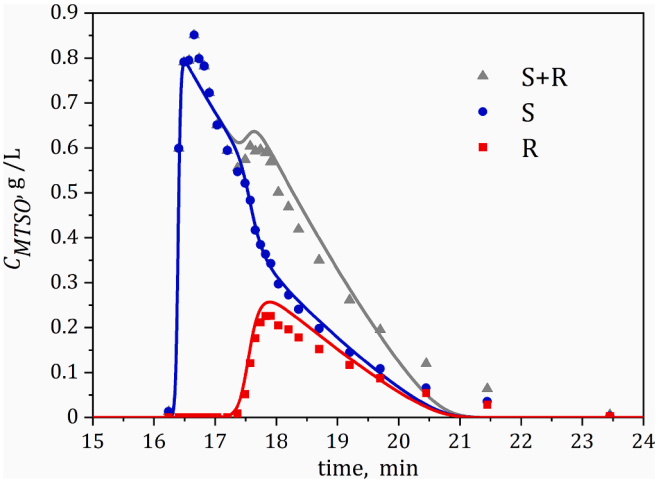

Fig. 3. Individual concentration profiles of *S* and *R*–MTSO enantiomers: symbols – experimental data, lines – results of peak fitting (separation condition provided in section 3.3.1). The parameters obtained from Eq. (3) are given in Table 1 (first row).

4.1.3. Selection and tuning of the operating variables

The model parameters determined in the batch column experiment were used for the simulation of ACh–SMB dynamics. To mimic the extension of the residence time of the mobile phase in the extra-column volume, the Henry constant was slightly increased by a proper change in the q^m value. That correction made only 0.5 % of the Henry constant value (Table 1, second row), since the contribution of the extra-column volume to the volume of the columns in the system was very small (section 3.3.2). The model was implemented in the random search optimization routine, which was used to select the operating variables for the ACh–SMB scouting run. The optimization was performed in two steps using two subsequent algorithms. In the first step, the set of dimensionless flowrates m^n ($n = 1,\ldots,4$) was optimized to maximize the purity of the target *S*–MTSO enantiomer at the raffinate outlet. Once the product purity, $Pu_{S,Ra}$, reached 99 % for the optimized set of m^n, the objective function $Pu_{S,Ra}$ was replaced by the productivity, $Pr_{S,Ra}$, and the second algorithm was subsequently activated, in which $Pr_{S,Ra}$, was maximized subject to the purity constraints, $Pu_{S,Ra} > 99$ %. The set of the optimized m^n values obtained was used to perform the scouting run (Table 2, run 1). The flowrates Q^2, Q^3, Q^4 and the switching time, t_{sw}, were calculated from the set of the optimized m^n values (Eq. 6) at the defined value of Q^1, which corresponded to the maximum flowrate allowed in the unit (section 3.3.2). These operating variables were subsequently changed in seven consecutive runs (Table 2, runs 2–8).

Separation of the enantiomers in the scouting run 1 was unsuccessful, as the total mass of the enantiomers delivered with the feed stream

Table 1
Isotherm coefficients estimated on the basis of the batch column experiments, used for the scouting run (run 1, Table 2) and adjusted on the basis of the reference run, REF (run 4, Table 2).

	K^I	q^m	K^{II}_{hom}	K^{II}_{het}
estimated for batch experiments	0.193	99.9	0.0213	0.0849
including extra-column volumes for run 1	0.193	100.4	0.0213	0.0849
adjusted based on run 4	0.193	100.4	0.0213	0.0891

Table 2
Operating variables used in different ACh–SMB runs. The value of $m^1 = 20.0$ determined for run 1 was kept for all consecutive runs.

Run	t_{sw}, min	m^2	m^3	m^4	ee_S, %	C_F, g/L
1 (scouting)	**7.0**	**4.5**	**12.6**	**9.8**	**50**	**5**
2	7.0	5.9	14.0	9.8	50	5
3	10.5	11.4	14.0	10.9	50	5
4 (REF)	**10.5**	**12.5**	**15.1**	**12.0**	**50**	**5**
5	10.5	12.5	15.1	12.0	30	5
6	10.5	12.5	15.1	12.0	70	5
7	10.5	12.5	15.1	12.0	50	3
8	10.5	12.5	15.1	12.0	50	7

Table 3
Performance indicators of the ACh–SMB runs 2–4 (Eqs. 19–22, $S \equiv E_1$). REF – the reference run (Table 2, run 4). $Pr_{S,Ra}$ is expressed in grams of *S*–MTSO, per liter of total column volume in the SMB unit (L_{col}) and per day.

Run	Goal of change	Y_S	$Pr_{S,Ra}$ g_S/(L_{col} day)	$Pu_{S,Ra}$	$\overline{C_{S,Ra}}$, g/L
2	Productivity improvement	14 %	66	90 %	1.0
3	Yield and purity improvement	26 %	28	100 %	0.9
4	REF	63 %	62	84 %	2.0

was collected at the extract outlet. This indicated that the concentration front of the target enantiomer migrated through the SMB unit slower than predicted by the ACh–SMB model; therefore, it did not reach the raffinate port (see Fig. 4, run 1). As described above, the model was calibrated based on the elution profiles recorded in a single experiment in the batch column at much lower loading volume compared to that used in the ACh–SMB process, therefore the accuracy of the prediction could not be expected to be perfect. However, since the entire mass of feed delivered was recovered at the extract outlet, the regeneration of the adsorbent in zone 1 was efficient. This implied that the isotherm slope, which determines the migration velocity of the rear part of the concentration profiles in zone 1, thus, in consequence the m^1 value, was correctly selected. In the subsequent trials that value was kept unchanged, whereas some of the remaining operating variables were tuned in runs 2, 3 and 4 to improve the process performance. The performance indicators obtained in these runs are reported in Table 3. Adjustments made and their purpose are visualized in Fig. 4, where the internal concentration profiles in the SMB unit are depicted using the model simulations. The unusual shape of the band profiles stems from the complexity of the SDE mechanism, which involves competition of enantiomers in multilayer adsorption.

To move the profiles of both enantiomers toward the raffinate outlet, the values of m^2 and m^3 were increased by the same value. After this adjustment was executed with adequate pumps, the experiment initiated by run 1 was continued in run 2 (Table 2) until a new steady state was established, which was verified by offline analysis of the concentration and purity of the outlet streams. The separation in run 2 turned out to be successful with respect to purity of the target enantiomer *S*–MTSO, but the productivity and yield of the separation were rather low (Table 3), since only a small volume of the pure *S*–MTSO fraction was collected at the raffinate outlet. To further improve the process performance, the values of m^4 and m^2 were increased. The latter caused the profiles of the enantiomers to move away from the extract outlet toward the raffinate outlet, whereas the former caused the volume of *S*–MTSO in the raffinate stream to increase. Additionally, to reduce the pressure drop in the SMB unit, the switching time was increased with an adequate decrease in flowrates in the SMB zones. The experiment was continued in run 3 (Table 2), in which an improvement in both yield and productivity was achieved with a very high purity ~ 100 % (Table 3). In the subsequent run 4, the values of m^2, m^3, m^4 were slightly increased to generate a reference run (Table 2, REF). It was intended that REF did not represent the best and optimized conditions with respect to productivity, yield,

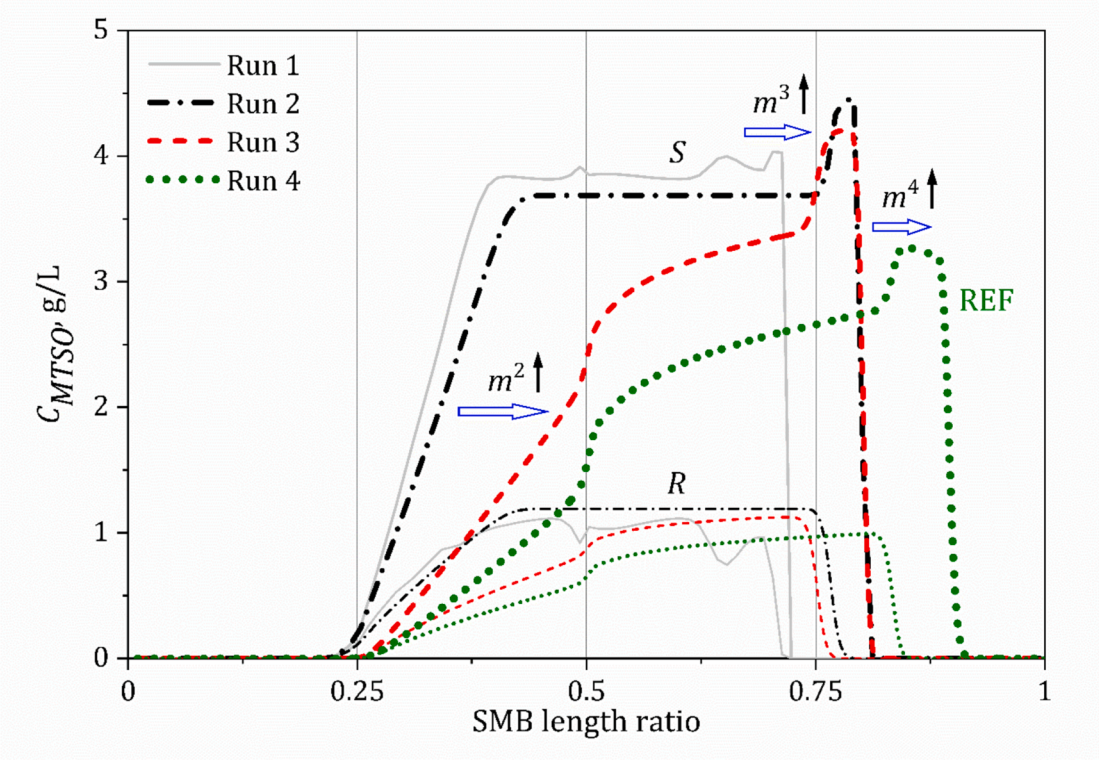

Fig. 4. Visualization of the predicted effect of tuning the operating variables in the ACh–SMB runs 1–4 on the course of the internal steady state profiles, which correspond to the end of the switch, $t = t_{sw}$. The model parameters used are given in Table 1 (third row).

and purity, but rather moderate ones. This allowed further analysis of positive and negative changes in process performance due to changes in other process parameters that were not considered before, though crucial for the separation performance, i.e., the total concentration of enantiomers and *ee* of the feed stream.

4.2. Influence of the total feed concentration and the ee of the feed

To investigate the influence of the concentration and ee_S of the feed stream, the last four runs (Table 2, runs 5–8) were performed, i.e., with increased and reduced concentrations or ee_S of the feed stream, keeping all remaining process variables the same as in run REF (Table 2, run 4). The effect of changes in the concentration and ee_S of the feed stream on the process performance is presented in Table 4. It is evident that increasing ee_S results in an improvement in purity; increasing the difference in the concentration of individual enantiomers causes an increase in the difference in the migration velocity of their fronts, which facilitates isolation of the pure enantiomer from the mixture. This is also visualized in Fig. 5, where a relatively narrow fraction of the pure product can be seen for the smallest $ee_S = 30$ % and much wider for $ee_S = 70$ %. Furthermore, increasing *ee* increases the mass ratio of the pure product to the unresolved waste fraction in the extract outlet, which improves the profitability of the method.

The effect of *ee* on yield depends on the isotherm range that corresponds to the concentration profiles of the enantiomers. In the range of strong isotherm nonlinearity, i.e., in the vicinity of the binding capacity, the front of the concentration profiles is very sharp, with almost vertical shape, whereas in the linear range it widens because of the enhanced contribution of kinetic effects to the retention mechanism, which particularly concerns the enantiomer that is depleted in the mixture. This makes the isolation of the target enantiomer fraction from the concentration fronts of unresolved fraction more challenging. This effect is most pronounced for run 6 ($ee_S = 70$ %), which is visualized in Fig. 5, where the changes in the shape of the concentration fronts of the enantiomers with the changes in ee_S are illustrated.

In general, increasing the concentration in the feed stream of the same *ee* enhances the SDE-effect, since it accelerates associate formation. Therefore, it is beneficial for the separation performance. However, the increased concentration triggers sharpening of the fronts of the profiles, for the same reason as discussed above. The high sensitivity of the position of the front of the band profile due to small changes in the process conditions renders the correct adjustment of process variables difficult, which may lead to purity reduction. The effect is visualized in Fig. 6. However, that issue can be mitigated by an online analysis of the band profiles and applying a control system to make sure that the front of the undesired enantiomer does not reach the raffinate port. It is evident that the concentration in the feed stream can be optimized for each specific case study to maximize the corresponding separation performance.

4.3. Verification of reproducibility and predictability of ACh–SMB

The separation results obtained in the REF run (run 4, Table 2) were used as a basis for the adjustment of the isotherm coefficients. The values of q^m and K^I, which characterize the adsorption on bare silica, were kept the same as determined from the batch experiment and used to design the scouting run (Table 1, second row). The difference between K^{II}_{hom} and K^{II}_{het}, which determine the separation selectivity, and thus the difference between the migration velocity of the concentration fronts of enantiomers along the column, was adjusted by fitting the predicted and experimental performance indicators, including the purity, yield and average concentrations of *S*–MTSO and *R*–MTSO at the raffinate outlet obtained in the REF run. The values of the isotherm coefficients obtained after the adjustment are reported in Table 1 (third row). The obtained K^{II}_{het} value was 5 % higher compared to that estimated from the batch experiment, whereas K^{II}_{hom} remained unchanged.

The corrected model was then used to predict the performance of the remaining runs 5–8 (Table 4). The agreement between the performance indicators predicted and experimentally obtained was satisfactory, which proved that the ACh–SMB process is predictable; hence, the mathematical model after proper calibration can be used for its design and optimization of the process conditions and the SMB configuration. The corresponding simulations of the internal SMB profiles are illustrated in Figs. 5 and 6.

The separation performance obtained for runs 4, 6 and 8 is comparable to the results reported in the literature for the separation of enantiomers by chiral chromatography, where the process productivity varied between 40 and 100 $g_S/(L_{col}\,day)$, and the eluent consumption between 8 and 10 L/g_S [22,47,48]. Finally, to verify the reproducibility of the measurements, some of the ACh–SMB runs were restarted. The results obtained in terms of performance indicators were very similar (maximum 2 % difference in product purity and maximum 10 % in product concentration), which confirmed the repeatability of the process (Supplementary materials, Table S1). The results reported above confirm the effectiveness of the ACh–SMB process and its applicability for industrial separation of enantiomers.

4.4. Application perspectives

The separation method developed in this study offers a cost-effective option for the separation of nonracemic mixtures with a high *ee*. Such mixtures are often an outcome of asymmetric synthesis. In this case, ACh–SMB can provide the target pure enantiomer with high productivity, as the amount of the target enantiomer in the extract stream containing the unresolved mixture, which is a process waste, is small compared to that received in the raffinate stream. In this case, complete elimination of expensive chiral chromatography may be economically very attractive. Furthermore, silica gel is not only significantly cheaper, but is also mechanically much more stable compared to CSPs. Therefore,

Table 4
Performance indicators (Eqs. (19–23)) of runs 4–8 (Table 2). Eluent consumption, EC, expressed in liters of solvent per gram of the product, $\overline{C_{S,Ra}}$, average concentration of the target enantiomer in the product stream (*Ra*), exp. – experimental data and sim. – model simulations.

Run	C_F/ee_s	Y_S		$Pr_{S,Ra}$ $g_S/(L_{col}\,day)$		$Pu_{S,Ra}$		$\overline{C_{S,Ra}}$ g/L		EC L/g_S	
		exp.	sim.	exp.	sim.	exp.	sim.	exp.	sim.	exp.	sim.
$C_F = 5$ g/L, ee_S changed											
5	**30 %**	45 %	44 %	39	39	73 %	72 %	1.2	1.7	6.6	4.8
***4**	**50 %**	63 %	63 %	62	62	84 %	84 %	2.0	2.0	4.1	4.1
6	**70 %**	54 %	53 %	61	60	96 %	94 %	1.9	2.3	4.2	3.4
C_F changed, $ee_S = 50$ %											
7	**3 g/L**	31 %	30 %	19	19	100 %	98 %	0.6	0.7	13.7	11.1
***4**	**5 g/L**	63 %	63 %	62	62	84 %	84 %	2.0	2.0	4.1	4.1
8	**7 g/L**	71 %	71 %	99	100	81 %	81 %	3.1	3.3	2.6	2.4

* Reference run was repeated in the table to better visualize the trends in changes in the performance indicators.

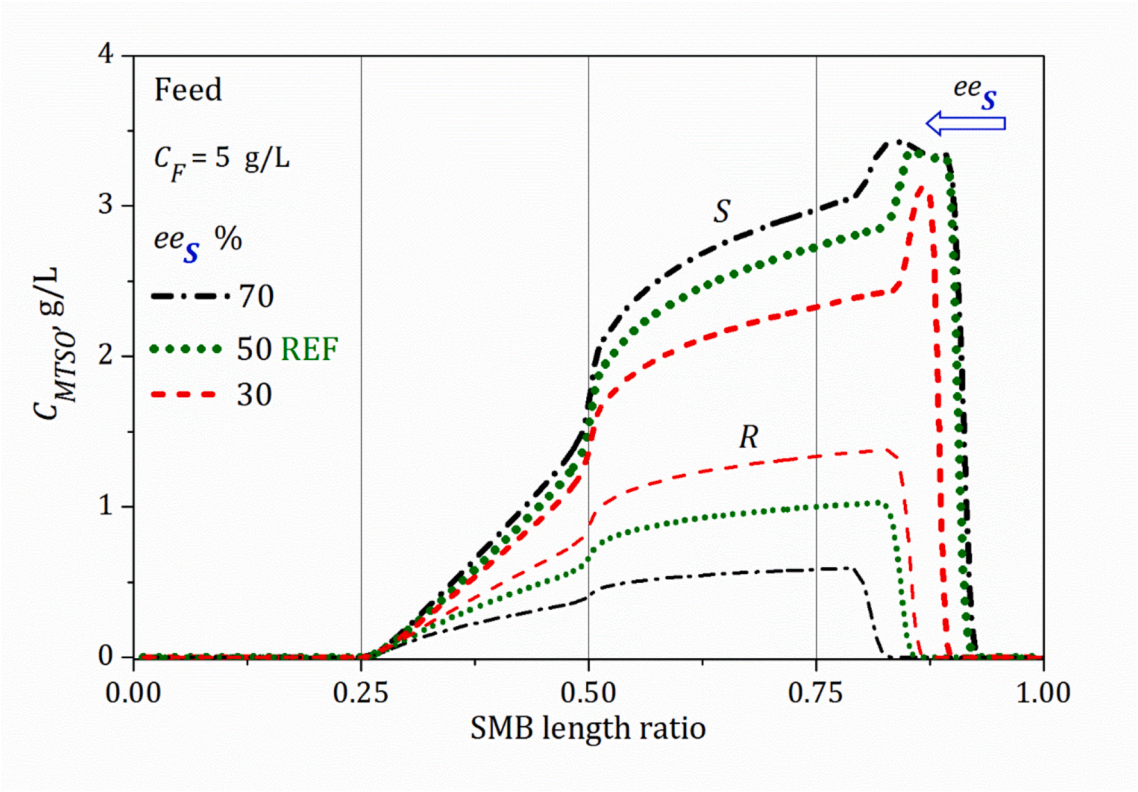

Fig. 5. Predicted effect of *ee* on the shape of the internal ACh–SMB profiles (steady state profiles at the end of the switch, $t = t_{sw}$). Runs 4 (REF), 5 and 6 (Table 2). Simulations with the isotherm parameters presented in Table 1 (third row).

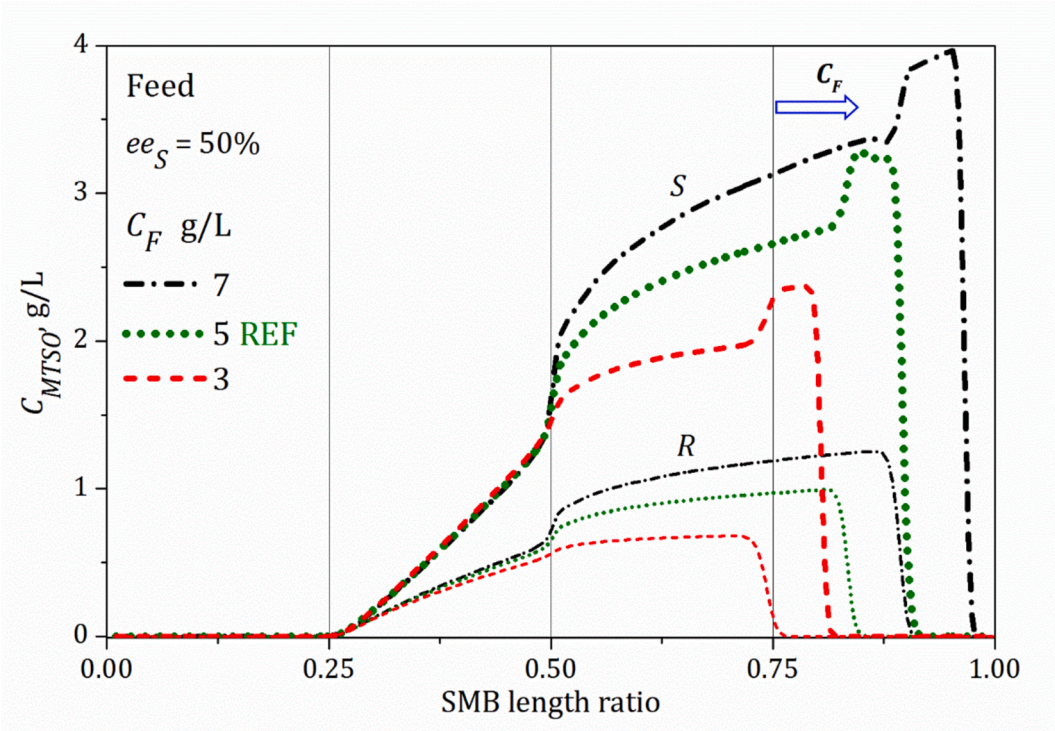

Fig. 6. Predicted effect of C_F on the shape and position of the internal ACh–SMB profiles. Runs 4 (REF), 7 and 8 (Table 2). Simulation conditions as in Fig. 5.

silica-packed beds can be operated under much higher column back pressure than CSP-packed beds. This allows the use of higher mobile phase flowrates to improve separation productivity.

For nonracemic mixtures with a low *ee*, the amount of waste stream at the extract outlet is high compared to the product stream, which can impair the process economy. However, the waste fraction can be further

processed by chiral chromatography to restore the initial *ee* and then recycled to ACh–SMB. Such a tandem configuration would allow for substantial reduction in the amounts of CSP required.

5. Conclusions

In this study, a concept of the achiral SMB process (ACh–SMB) was developed for the isolation of the target enantiomer from nonracemic mixtures. The concept was verified for a model mixture of methyl *p*–tolyl sulfoxide (MTSO) enantiomers that was separated in a normal phase system using a bare silica gel adsorbent. The separation was driven by the SDE phenomenon, which allowed isolation of the target enantiomer (*S*–MTSO) present in excess of nonracemic mixtures.

The preliminary stage of the process design consisted of the formulation of a mass balance based model of the process dynamics, which accounted for the specificity of the SDE-driven separation, and its calibration on the basis of individual profiles of enantiomers measured in the batch column experiment. The model simulations were used to select operating variables, i.e., the zone flowrates and the switching time, to perform a first ACh-SMB scouting run. To improve process performance, these variables were subsequently adjusted in the next three SMB runs. In the most successful run, the product with approximately 100 % purity and productivity of 28 g_S per column volume per day was obtained. Furthermore, a reference run was evaluated to investigate the effects exerted by changes in other relevant process variables, including the concentration and enantiomeric excess (ee_S) of the feed stream.

In general, the increase in the feed *ee* enhanced the process productivity as a result of increasing the difference in the migration velocity of the enantiomers along the columns. An increase in the feed concentration enhanced the SDE effect, which was beneficial for the process performance, but on the other hand, it made maintaining the product purity at the appropriate level more difficult. The effects observed could be reproduced by the dynamic model developed.

The results achieved reveal that the developed process is feasible, predictable, and reproducible. Furthermore, productivity and eluent consumption were in a range similar to those reported in the literature for chiral separations. However, the material costs for achiral chromatographic separations are significantly lower. Therefore, the ACh–SMB technique has the potential to be applied in large-scale industrial separation as a stand-alone operation or in combination with a chiral separation method. The process can be particularly efficient in the separation of nonracemic mixtures with a high enantiomeric excess, for which a great amount of pure target enantiomer can be isolated from the feed mixture. Obviously, the technique is exclusively feasible for chiral compounds that contain SDE-phoric groups or can be functionalized with those groups.

A more detailed study is underway for better characterization and optimization of the process and the system configuration. The concept of coupling ACh–SMB with a chiral separation technique will also be investigated.

Declaration of competing interest

The authors declare that they have no known competing financial interests or personal relationships that could have appeared to influence the work reported in this paper.

Acknowledgement

Financial support of this work by National Science Centre (UMO–2021/41/B/ST8/00631) is gratefully acknowledged.

Appendix A. Supplementary data

Supplementary data to this article can be found online at https://doi.org/10.1016/j.seppur.2025.131497

Research data for this article

Mendeley Data base: https://doi.org/10.17632/nnmttw6v6r.1.

References

[1] J. Sui, N. Wang, J. Wang, X. Huang, T. Wang, L. Zhou, H. Hao, Strategies for chiral separation: from racemate to enantiomer, Chem. Sci. 14 (2023) 11955–12003, https://doi.org/10.1039/D3SC01630G.
[2] FDA'S policy statement for the development of new stereoisomeric drugs, Chirality 4 (1992) 338–340. https://doi.org/10.1002/chir.530040513.
[3] I. Agranat, H. Caner, Intellectual property and chirality of drugs, Drug Discov. Today 4 (1999) 313–321, https://doi.org/10.1016/S1359-6446(99)01363-X.
[4] I. Agranat, H. Caner, J. Caldwell, Putting chirality to work: the strategy of chiral switches, Nat. Rev. Drug Discov. 1 (2002) 753–768, https://doi.org/10.1038/nrd915.
[5] A. Calcaterra, I. D'Acquarica, The market of chiral drugs: Chiral switches versus de novo enantiomerically pure compounds, J. Pharm. Biomed. Anal. 147 (2018) 323–340, https://doi.org/10.1016/j.jpba.2017.07.008.
[6] G. Hancu, A. Modroiu, Chiral Switch: Between Therapeutical Benefit and Marketing Strategy, Pharmaceuticals 15 (2022), https://doi.org/10.3390/ph15020240.
[7] R.U. McVicker, N.M. O'Boyle, Chirality of New Drug Approvals (2013–2022): Trends and Perspectives, J. Med. Chem. 67 (2024) 2305–2320, https://doi.org/10.1021/acs.jmedchem.3c02239.
[8] K. Matheis, M. Granvogl, P. Schieberle, Quantitation and Enantiomeric Ratios of Aroma Compounds Formed by an Ehrlich Degradation of l-Isoleucine in Fermented Foods, J. Agric. Food Chem. 64 (2016) 646–652, https://doi.org/10.1021/acs.jafc.5b05427.
[9] P. Jeschke, Current status of chirality in agrochemicals, Pest Manag. Sci. 74 (2018) 2389–2404, https://doi.org/10.1002/ps.5052.
[10] Eric Francotte, Wolfgang Lindner, Chirality in Drug Research, Wiley-VCH Verlag GmbH & Co. KGaA, n.d.
[11] James P. Riehl., Mirror-Image Asymmetry: An Introduction to the Origin and Consequences of Chirality., n.d.
[12] S. Wu, R. Snajdrova, J.C. Moore, K. Baldenius, U.T. Bornscheuer, Biocatalysis: Enzymatic Synthesis for Industrial Applications, Angew. Chem. Int. Ed. 60 (2021) 88–119, https://doi.org/10.1002/anie.202006648.
[13] S. Peng, Y. Zhu, C. Luo, P. Zhang, F. Wang, R. Li, G. Lin, J. Zhang, Chiral drugs: Sources, absolute configuration identification, pharmacological applications, and future research trends, LabMed Discovery (2024) 100008, https://doi.org/10.1016/j.lmd.2024.100008.
[14] H. Caner, E. Groner, L. Levy, I. Agranat, Trends in the development of chiral drugs, Drug Discov. Today 9 (2004) 105–110, https://doi.org/10.1016/S1359-6446(03)02904-0.
[15] T.J. Ward, K.D. Ward, Chiral Separations: A Review of Current Topics and Trends, Anal. Chem. 84 (2012) 626–635, https://doi.org/10.1021/ac202892w.
[16] H. Lorenz, A. Seidel-Morgenstern, Processes To Separate Enantiomers, Angew. Chem. Int. Ed. 53 (2014) 1218–1250, https://doi.org/10.1002/anie.201302823.
[17] J.-H. Zhang, S.-M. Xie, L.-M. Yuan, Recent progress in the development of chiral stationary phases for high-performance liquid chromatography, J. Sep. Sci. 45 (2022) 51–77, https://doi.org/10.1002/jssc.202100593.
[18] A. Collet, M.J. Brienne, J. Jacques, Optical resolution by direct crystallization of enantiomer mixtures, Chem. Rev. 80 (1980) 215–230, https://doi.org/10.1021/cr60325a001.
[19] M. Mazzotti, G. Storti, M. Morbidelli, Robust design of countercurrent adsorption separation processes: 2. Multicomponent systems, AIChE Journal 40 (1994) 1825–1842, https://doi.org/10.1002/aic.690401107.
[20] M. Mazzotti, G. Storti, M. Morbidelli, Robust design of countercurrent adsorption separation: 3. Nonstoichiometric systems, AIChE Journal 42 (1996) 2784–2796, https://doi.org/10.1002/aic.690421010.
[21] M. Mazzotti, G. Storti, M. Morbidelli, Optimal operation of simulated moving bed units for nonlinear chromatographic separations, J. Chromatogr. A 769 (1997) 3–24, https://doi.org/10.1016/S0021-9673(97)00048-4.
[22] R.S. Arafah, A.E. Ribeiro, A.E. Rodrigues, L.S. Pais, Improving the performance of nadolol stereoisomers' preparative separation using Chiralpak IA by SMB chromatography, Chirality 31 (2019) 62–71, https://doi.org/10.1002/chir.23034.
[23] D.C.S. Azevedo, L.S. Pais, A.E. Rodrigues, Enantiomers separation by simulated moving bed chromatography: Non-instantaneous equilibrium at the solid–fluid interface, J. Chromatogr. A 865 (1999) 187–200, https://doi.org/10.1016/S0021-9673(99)00990-5.
[24] R. Calderón Supelano, A.G. Barreto, A.R. Secchi, Optimal performance comparison of the simulated moving bed process variants based on the modulation of the length of zones and the feed concentration, J. Chromatogr. A (1651 (2021)) 462280, https://doi.org/10.1016/j.chroma.2021.462280.
[25] F.C. Cunha, A.R. Secchi, M.B. de Souza Jr, A.G. Barreto Jr, Separation of praziquantel enantiomers using simulated moving bed chromatographic unit with performance designed for semipreparative applications, Chirality 31 (2019) 583–591, https://doi.org/10.1002/chir.23084.
[26] A.C. da Silva Jr, A.G. Salles Jr, R.F. Perna, C.R. Correia, C.C. Santana, Chromatographic Separation and Purification of Mitotane Racemate in a Varicol Multicolumn Continuous Process, Chemical Engineering & Technology 35 (2012) 83–90, https://doi.org/10.1002/ceat.201100209.

[27] X. Jiang, L. Zhu, B. Yu, Q. Su, J. Xu, W. Yu, Analyses of simulated moving bed with internal temperature gradients for binary separation of ketoprofen enantiomers using multi-objective optimization: Linear equilibria, J. Chromatogr. A 1531 (2018) 131–142, https://doi.org/10.1016/j.chroma.2017.11.045.
[28] X. Lin, R. Gong, J. Li, P. Li, J. Yu, A.E. Rodrigues, Enantioseparation of racemic aminoglutethimide using asynchronous simulated moving bed chromatography, J. Chromatogr. A 1467 (2016) 347–355, https://doi.org/10.1016/j.chroma.2016.08.031.
[29] M. Pedeferri, G. Zenoni, M. Mazzotti, M. Morbidelli, Experimental analysis of a chiral separation through simulated moving bed chromatography, Chem. Eng. Sci. 54 (1999) 3735–3748, https://doi.org/10.1016/S0009-2509(99)00031-7.
[30] A. Rajendran, G. Paredes, M. Mazzotti, Simulated moving bed chromatography for the separation of enantiomers, J. Chromatogr. A 1216 (2009) 709–738, https://doi.org/10.1016/j.chroma.2008.10.075.
[31] Y. Zhang, K. Hidajat, A.K. Ray, Multi-objective optimization of simulated moving bed and Varicol processes for enantio-separation of racemic pindolol, Sep. Purif. Technol. 65 (2009) 311–321, https://doi.org/10.1016/j.seppur.2008.10.050.
[32] V.A. Soloshonok, Remarkable Amplification of the Self-Disproportionation of Enantiomers on Achiral-Phase Chromatography Columns, Angew. Chem. Int. Ed. 45 (2006) 766–769, https://doi.org/10.1002/anie.200503373.
[33] P. Diter, S. Taudien, O. Samuel, H.B. Kagan, Enantiomeric enrichment of sulfoxides by preparative flash chromatography on an achiral phase, J. Org. Chem. 59 (1994) 370–373, https://doi.org/10.1021/jo00081a015.
[34] E. Gil-Av, V. Schurig, Resolution of non-racemic mixtures in achiral chromatographic systems: A model for, the enantioselective effects observed, J. Chromatogr. A 666 (1994) 519–525, https://doi.org/10.1016/0021-9673(94)80413-3.
[35] R.-M. Nicoud, J.-N. Jaubert, I. Rupprecht, J. Kinkel, Enantiomeric enrichment of non-racemic mixtures of binaphthol with non- chiral packings, Chirality 8 (1996) 234–243, https://doi.org/10.1002/(SICI)1520-636X(1996)8:3<234::AID-CHIR2>3.0.CO;2-H.
[36] V.A. Soloshonok, H. Ueki, M. Yasumoto, S. Mekala, J.S. Hirschi, D.A. Singleton, Phenomenon of Optical Self-Purification of Chiral Non-Racemic Compounds, J. Am. Chem. Soc. 129 (2007) 12112–12113, https://doi.org/10.1021/ja065603a.
[37] A.E. Sorochinsky, V.A. Soloshonok, Self-disproportionation of enantiomers of enantiomerically enriched compounds, Differentiation of enantiomers II (2013) 301–339.
[38] J. Han, V.A. Soloshonok, K.D. Klika, J. Drabowicz, A. Wzorek, Chiral sulfoxides: advances in asymmetric synthesis and problems with the accurate determination of the stereochemical outcome, Chem. Soc. Rev. 47 (2018) 1307–1350, https://doi.org/10.1039/C6CS00703A.
[39] J. Han, A. Wzorek, V.A. Soloshonok, K.D. Klika, The self-disproportionation of enantiomers (SDE): The effect of scaling down, potential problems versus prospective applications, possible new occurrences, and unrealized opportunities? Electrophoresis 40 (2019) 1869–1880, https://doi.org/10.1002/elps.201800414.
[40] M. Kwiatkowska, A. Wzorek, A. Kolbus, M. Urbaniak, J. Han, V.A. Soloshonok, K. D. Klika, Flurbiprofen: A Study of the Behavior of the Scalemate by Chromatography, Sublimation, and NMR, Symmetry 13 (2021), https://doi.org/10.3390/sym13040543.
[41] S. Mazzotta, V. Rositano, L. Senaldi, A. Bernardi, P. Allegrini, G. Appendino, Scalemic natural products, Nat. Prod. Rep. 40 (2023) 1647–1671, https://doi.org/10.1039/D3NP00014A.
[42] M. Olbrycht, J. Gumieniak, P. Mruc, M. Balawejder, W. Piątkowski, D. Antos, Separation of non-racemic mixtures of enantiomers by achiral chromatography, J. Chromatogr. A 1693 (2023) 463877, https://doi.org/10.1016/j.chroma.2023.463877.
[43] P. Mruc, M. Olbrycht, M. Korbetskyy, D. Antos, Altering the mobile phase composition to enhance self-disproportionation of enantiomers in achiral chromatography, J. Chromatogr. A 1715 (2024) 464603, https://doi.org/10.1016/j.chroma.2023.464603.
[44] G.A. Guiochon, A. Felinger, A. Katti, D.G. Shirazi, Fundamentals of preparative and nonlinear chromatography, Elsevier, Amsterdam, Netherlands, United States, 2006. https://www.osti.gov/biblio/989603.
[45] P. Rouchon, M. Schonauer, P. Valentin, G. Guiochon, Numerical Simulation of Band Propagation in Nonlinear Chromatography, Sep. Sci. Technol. 22 (1987) 1793–1833, https://doi.org/10.1080/01496398708057614.
[46] H. Kniep, G. Mann, C. Vogel, A. Seidel-Morgenstern, Separation of Enantiomers through Simulated Moving-Bed Chromatography, Chem. Eng. Technol. 23 (2000) 853–857, https://doi.org/10.1002/1521-4125(200010)23:10<853::AID-CEAT853>3.0.CO;2-2.
[47] J. Matos, R.P.V. Faria, J.M. Loureiro, A.M. Ribeiro, I.B.R. Nogueira, Optimal Design of SMB Units: A Novel Strategy Based on Particles Swarm Optimization, IFAC-PapersOnLine 54 (2021) 548–553, https://doi.org/10.1016/j.ifacol.2021.08.299.
[48] X. Zhang, J. Liu, A.K. Ray, Y. Li, Research Progress on the Typical Variants of Simulated Moving Bed: From the Established Processes to the Advanced Technologies, Processes 11 (2023), https://doi.org/10.3390/pr11020508.